Journal of Electronic Materials (2021) 50:6941–6950
https://doi.org/10.1007/s11664-021-09258-z

ORIGINAL RESEARCH ARTICLE

Titanium-Doped Nickel-Rich Layered $LiNi_{0.8}Co_{0.2}O_2$ as High-Performance Cathode Material for Lithium-Ion Batteries

Xiaohong Zhang[1] · Mingcan Wang[1] · Jiayuan Shi[1] · Xiaotao Chen[1] · Fuliang Liu[1] · Bin Shi[1]

Received: 6 April 2021 / Accepted: 23 September 2021 / Published online: 13 October 2021

Abstract

$LiNi_{0.8}Co_{0.2-x}Ti_xO_2$ cathode materials with different titanium (Ti) contents have been prepared from $Ni_{0.8}Co_{0.2-x}Ti_x(OH)_2$ ($0 \le x \le 0.05$) precursors. Phase and morphology analyses indicated that the products were microspheres in space group *R3m* assembled from smaller secondary particles. Phase and elemental analyses indicated more serious cation mixing in the layered materials obtained with Ti doping. The $LiNi_{0.8}Co_{0.2-x}Ti_xO_2$ material with $x = 0.0125$ showed optimal electrochemical performance with improved cycling performance (capacity retention ratio of 95.8% after 100 cycles) and high rate capability (162 mAh g^{-1} at 2C). Therefore, Ti doping can be considered an efficient approach to improve the electrochemical properties of such cathode materials.

Keywords $LiNi_{0.8}Co_{0.2-x}Ti_xO_2$ · nickel-rich · titanium doping · lithium-ion batteries · cathode materials

Introduction

Lithium-ion batteries (LIBs) have been widely used as electrochemical energy storage devices in many fields including portable electronics, electric vehicles, and energy storage systems because of their outstanding advantages such as light weight, long cycle life, and low cost.[1,2] However, the relatively low discharge capacity of traditional commercialized LIB cathode materials such as olivine $LiFePO_4$, layered $LiCoO_2$, and spinel $LiMn_2O_4$ has greatly limited their industrial application and relevant device performance.[3] Compared with traditional $LiCoO_2$ material, the layered solid solution $LiNi_xCo_{1-x}O_2$ ($0 < x < 1$) has been reported to be one of the potential alternative candidates due to its higher capacity and lower cost.[4,5] The utilization of lithium ions in the intercalation and deintercalation processes is higher in $LiNi_xCo_{1-x}O_2$ materials, especially $LiNi_{0.8}Co_{0.2}O_2$, than in $LiCoO_2$ material.[6,7]

Many different methods have been reported for synthesis of $LiNi_{0.8}Co_{0.2}O_2$ microstructures, including room-temperature growth,[8] the sol–gel method,[9] emulsion drying,[10] coprecipitation,[11] and the hydrothermal approach.[12] Particle size control, precursor selection, and the thin-film technique have significant effects on the electrochemistry of $LiNi_{0.8}Co_{0.2}O_2$ cathodes.[3,13–15] Nevertheless, the electrochemical stability of these Ni-rich layered oxides remains poor due to surface degradation, gas release, and cation mixing of $LiNi_{0.8}Co_{0.2}O_2$ structures during electrochemical cycling.[16–18] To solve these problems, surface modification with MgO and coating with Li_2ZrO_3 on $LiNi_{0.8}Co_{0.2}O_2$ have been reported to improve the structural stability.[19,20] Metal doping has also been studied for $LiNi_{0.8}Co_{0.2}O_2$ modification; For example, Nb^{5+} doping at Li^+ sites in the $LiNi_{0.8}Co_{0.2}O_2$ crystal lattice resulted in an acceleration of lithium-ion migration and an enhancement of the high-rate performance.[21] Doping of size-invariant Zn^{2+} into $LiNi_{0.8}Co_{0.2}O_2$ structures decreased the polarization and improved the reversibility of the redox processes during cycling.[22]

Titanium (Ti) doping has been considered as an efficient approach to improve the electrochemical properties of cathode materials including $Li_3V_2(PO_4)_3$,[23] Li_2FeSiO_4,[24] $Li_3Fe_2(PO_4)_3$,[25] and layered metal oxide. Ti doping creates cation vacancies in the crystal structure that can improve the electronic conductivity and ionic diffusion of cathode materials.[26] The electrochemical inactivity of Ti^{4+} increased the structural stability of the cathode and inhibited crack formation in the crystal structure during electrochemical

✉ Jiayuan Shi
jiayshi@163.com

[1] State Key Laboratory of Advanced Chemical Power Sources (SKL-ACPS), Guizhou Meiling Power Sources Co., Ltd., Zunyi 563003, Guizhou, People's Republic of China

cycling.[24,27] For $LiNi_{0.80}Co_{0.15}Al_{0.05}O_2$ cathodes, Ti substitution at Co sites can suppress the phase transformation during charging.[28,29] For $LiNi_{0.8}Co_{0.1}Mn_{0.1}O_2$ cathodes, Ti doping reduced the cation mixing between Li^+ and Ni^{2+} through the pillar effect, which favors capacity retention.[30,31] For $LiNi_{0.8}Co_{0.2}O_2$ cathodes, Liu's group[32] and Zhang's group[33] reported Ti doping of $LiNi_{0.8}Co_{0.2}O_2$ by using $Ni_xCo_y(OH)_z$ as the precursor. The Ti doping process was carried out through calcination of $Ni_xCo_y(OH)_z$ in presence of LiOH and Ti precursor. However, Ti species mainly appeared on the particle surfaces. Uniform distribution of Ti element in $LiNi_{0.8}Co_{0.2}O_2$ particles cannot be ensured but is important to improve the structural stability and ion diffusion in the $LiNi_{0.8}Co_{0.2}O_2$ particles.

In the work described herein, $Ni_{0.8}Co_{0.2-x}Ti_x(OH)_2$ was prepared by the coprecipitation method and served as the precursor for $LiNi_{0.8}Co_{0.2-x}Ti_xO_2$ ($0 < x \leq 0.05$) cathode materials. The crystallinity and surface morphology of Ni-enriched materials can be significantly affected by Ti doping, as indicated by x-ray diffraction (XRD) analysis and scanning electron microscopy (SEM) analysis, respectively. Electrochemical testing of $LiNi_{0.8}Co_{0.2-x}Ti_xO_2$ ($0 < x \leq 0.05$) was carried out to study the influence of the Ti doping on the cycling stability and rate performance of the $LiNi_{0.8}Co_{0.2}O_2$ cathode. The electrochemical reversibility and ionic conductivity of the $LiNi_{0.8}Co_{0.2-x}Ti_xO_2$ cathodes were studied by using cyclic voltammetry (CV) and electrochemical impedance spectroscopy (EIS) tests.

Experimental Procedures

Synthesis

$Ni_{0.8}Co_{0.2-x}Ti_x(OH)_2$ precursors were obtained by the coprecipitation method. Firstly, $NiSO_4{\cdot}6H_2O$, $CoSO_4{\cdot}7H_2O$, and $TiOSO_4{\cdot}8H_2O$ were dissolved in water together in argon with the total concentration of Ni, Co, and Ti in the polymetallic solution fixed at 2 mol L^{-1}. The molar ratio of Ni and Co to Ti was $0.8:(0.2-x):x$ ($x = 0$, 0.0125, 0.025, and 0.05). NaOH solution (4 mol L^{-1}) and ammonia (28 wt%) were mixed at volume ratio of 10:1 as the alkaline solution. Then, the pH of the polymetallic solution was adjusted to 11.3 ± 0.05 using a water bath at 55°C by adding the alkaline solution dropwise in argon. After aging for 12 h, the obtained $Ni_{0.8}Co_{0.2-x}Ti_x(OH)_2$ precipitate was filtered, washed with deionized water repeatedly, and dried at 100°C for 24 h. Thereafter, the $Ni_{0.8}Co_{0.2-x}Ti_x(OH)_2$ precipitate was sintered together with $LiOH{\cdot}H_2O$ at molar ratio of 1:1.1 at 550°C in air for 5 h then calcined at 750°C in oxygen for 12 h. Finally, $LiNi_{0.8}Co_{0.2-x}Ti_xO_2$ ($x = 0$, 0.0125, 0.025, and 0.05) cathode materials were obtained after grinding and screening. The samples with x values of 0, 0.0125, 0.025, and 0.05 are denoted as LNCTO-0, LNCTO-1.25, LNCTO-2.5, and LNCTO-5, respectively.

Characterization

The crystalline structure of the prepared materials was characterized by powder x-ray diffraction (XRD) analysis (PANalytical X'Pert Powder) measurement using Cu K_α radiation in the 2θ range from 10° to 90° with step size of 0.02°. Rietveld refinement was carried out by using the TOPAS 5 software package to obtain the lattice parameters. Morphological studies of the prepared samples were carried out by scanning electron microscopy (SEM, JEOL, JSM-7800F). Energy-dispersive spectroscopy (EDS) was employed in SEM to investigate the distribution of the elements. x-Ray photoelectron spectroscopy (XPS, ESCALab250) was employed to determine the elemental distribution of the materials. The actual content of Ti, Ni, and Co elements in each product was determined by inductively coupled plasma optical emission spectroscopy (AGILENT ICP-OES 730).

Electrochemical Measurements

$LiNi_{0.8}Co_{0.2-x}Ti_xO_2$ powders were mixed with polyvinylidene fluoride as binder and super P as conductor at mass ratio of 90%:5%:5% in *N*-methyl-2-pyrrolidone (NMP). The mixed slurry was coated uniformly on aluminum foil and dried at 120°C for 10 h in vacuum. The electrochemical performance of $LiNi_{0.8}Co_{0.2-x}Ti_xO_2$ was evaluated by using CR2032 coin cells with lithium metal as reference electrode and Celgard 2300 as separator. $LiPF_6$ (1 M) in ethylene carbonate (EC)/ethylmethyl carbonate (EMC)/dimethyl carbonate (DMC) (1:1:1 v/v/v) was used as electrolyte. Electrochemical measurements were performed between 2.5 V and 4.3 V (versus Li/Li^+) using a Neware test instrument. Cyclic voltammetry (CV) measurements were carried on an electrochemical workstation (CHI660C, Shanghai Chenhua) at scan rate of 0.1 mV s^{-1} between 3.0 V and 4.6 V (versus Li/Li^+). Electrochemical impedance spectroscopy (EIS) tests were performed at full charged state after cycling in the frequency range of 0.001 Hz to 100 kHz by applying an alternating-current (AC) amplitude of 5 mV on a CHI660C electrochemical workstation.

Results and Discussion

The XRD patterns of four $LiNi_{0.8}Co_{0.2-x}Ti_xO_2$ samples are shown in Fig. 1a. All the diffraction peaks of the four samples can be indexed to the layered α-$NaFeO_2$ structure in space group $R\bar{3}m$ (Fig. 1a).[34,35] No peaks corresponding to TiO_2 or other impurity phases were observed, indicating the high purity of the obtained α-$NaFeO_2$ phase in the four

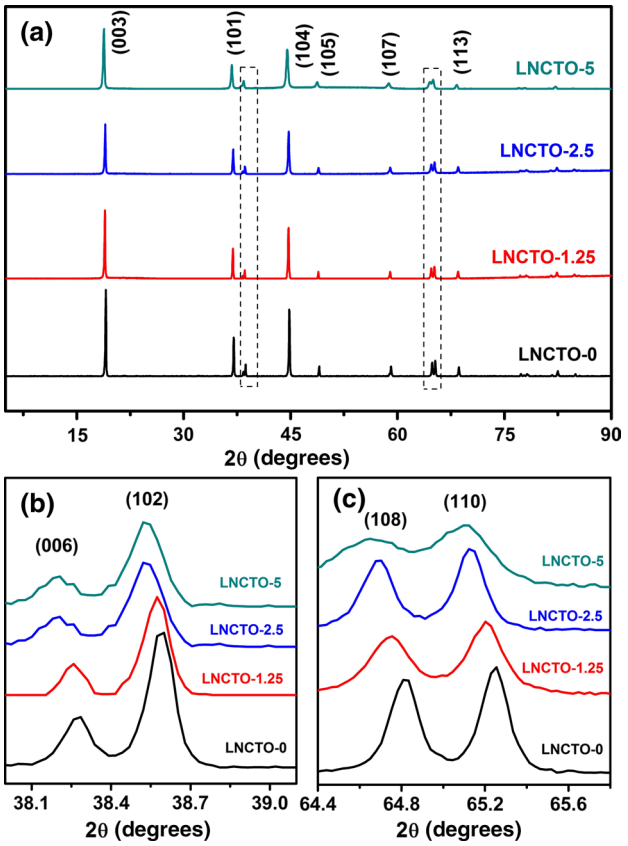

Fig. 1 (a) XRD patterns of $LiNi_{0.8}Co_{0.2-x}Ti_xO_2$ samples and partial enlargements of (b) (006)/(102) and (c) (108)/(110) doublets.

samples. Two portions of the XRD patterns marked by dotted boxes in Fig. 1a are shown enlarged in Fig. 1b, c. Clear splitting of both (006)/(012) and (108)/(110) doublets can be observed in Fig. 1b, c for all four samples, indicating the well-developed structural ordering of the obtained Ni-rich layered materials.[36,37]

To investigate the influence of Ti doping on the crystal structure of $LiNi_{0.8}Co_{0.2}O_2$, the lattice constants and other structural parameters were calculated and are summarized in Fig. 2 and Table I. The high *c*/*a* value of $LiNi_{0.8}Co_{0.2}O_2$ (> 4.94) indicates its layered structure. Moreover, compared with $LiNi_{0.8}Co_{0.2}O_2$, the increase of the *c*/*a* value found for the three $LiNi_{0.8}Co_{0.2-x}Ti_xO_2$ samples indicates an improvement of the layered crystal structure upon Ti doping of $LiNi_{0.8}Co_{0.2}O_2$.[38,39] The $I(003)/I(104)$ values of the samples decreased with increasing Ti doping amount, demonstrating the more serious Li^+/Ni^{2+} cation mixing in layered materials after Ti doping.[40,41] In addition, the cell volumes were slightly enlarged upon Ti doping of $LiNi_{0.8}Co_{0.2}O_2$, leading to enlarged Li-ion transport channels and improved lithium diffusion in Ti-doped crystal structures.[31] However, excessive Ti in the $LiNi_{0.8}Co_{0.2-x}Ti_xO_2$ materials may result in a reduction of the reversible capacity because of the electrochemical inertness of Ti^{4+} ions.[42,43]

The morphology and microstructure of the $LiNi_{0.8}Co_{0.2-x}Ti_xO_2$ ($0 \le x \le 0.05$) samples were observed by SEM; typical images are shown in Fig. 3. All four samples were composed of microspheres with size from several to more than ten micrometers. All the microspheres were assembled from smaller secondary particles, and some spheres were connected together. Many pores could be observed among adjacent secondary particles, providing space for sufficient contact with the electrolyte.[32,40] When the *x* values was changed from 0 to 0.025, the size of the secondary particles could be controlled in the range from 0.2 μm to 1.5 μm (Fig. 3a–f). However, when *x* reached 0.05, the secondary particles were larger than 3 μm (Fig. 3g, h). This indicates that the morphology of $LiNi_{0.8}Co_{0.2-x}Ti_xO_2$ with low Ti doping amounts (≤ 0.025) may be similar to that of $LiNi_{0.8}Co_{0.2}O_2$, while excess Ti in the crystal (≥ 0.05) had a significant effect on the structure of $LiNi_{0.8}Co_{0.2-x}Ti_xO_2$.

Taking LNCTO-1.25 as an example, EDX elemental analysis was carried out to study the distribution of O, Ni, Co, and Ti elements in the square region of the Ti-doped particle (Fig. 4). The mapping result for Ti element completely overlapped with those of O, Ni, and Co elements, indicating a homogeneous distribution of Ti element in the Ti-doped $LiNi_{0.8}Co_{0.2}O_2$ samples.

To compare the surface elemental composition and valence states of the $LiNi_{0.8}Co_{0.2-x}Ti_xO_2$ samples, LNCTO-0 and LNCTO-1.25 were chosen for XPS tests; their corresponding spectra are shown in Fig. 5. Both XPS results show characteristic peaks near 55 eV, indicating presence of Li element in the two samples (Fig. 5a). However, only LNCTO-1.25 showed peaks at 457.3 eV and 463.0 eV, which can be assigned to Ti $2p_{3/2}$ and Ti $2p_{1/2}$, indicating presence of Ti^{4+} in LNCTO-1.25 upon Ti doping (Fig. 5b).[44] The Ni 2*p* spectrum contained two peaks at 855.0 eV (Ni $2p_{3/2}$) and 872.67 eV (Ni $2p_{1/2}$), and the splitting of the Ni $2p_{3/2}$ peak can be assigned to Ni^{3+} (855.83 eV) and Ni^{2+} (854.75 eV) (Fig. 5c).[45] Compared with LNCTO-0, the ratio of Ni^{2+} to Ni^{3+} was significantly increased for LNCTO-1.25, indicating more serious Li^+/Ni^{2+} mixing upon Ti doping.[20] This is consistent with the XRD results, and proper cation mixing can enhance the structural stability of layered cathode materials.[46] The peaks observed near 861 eV and 880 eV in the Ni 2*p* spectrum can be attributed to satellites of Ni $2p_{3/2}$ and Ni $2p_{1/2}$, respectively.[31] The binding energies of 780 eV and 794.9 eV correspond to Co $2p_{3/2}$ and Co $2p_{1/2}$, respectively (Fig. 5d). The splitting of the Co $2p_{3/2}$ peak indicates a mixed valence state of Co^{2+} with Co^{3+} in these two samples.[47] Compared with LNCTO-0, the ratio of Co^{2+} to Co^{3+} was higher for LNCTO-1.25, which may be because of the charge equilibrium in the presence of Ti^{4+}.[48]

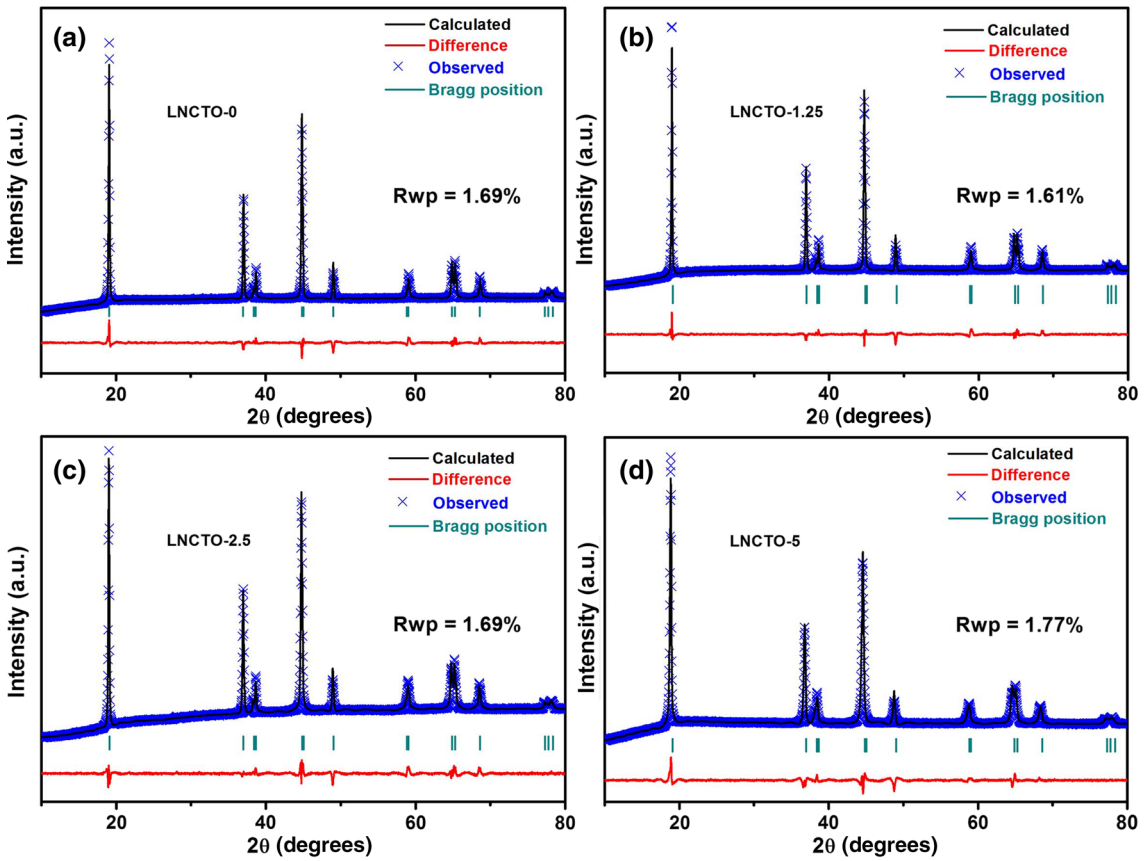

Fig. 2 Rietveld refinement results of XRD data for (a) LNCTO-0, (b) LNCTO-1.25, (c) LNCTO-2.5, and (d) LNCTO-5.

Table I Cell parameters and composition of $LiNi_{0.8}Co_{0.2-x}Ti_xO_2$ samples

Sample	*a* (Å)	*c* (Å)	*V* (Å^3)	*c*/*a*	*I*(003)/*I*(104)	Molar Ratio (Ni/Co/Ti)
LNCTO-0	2.8648	14.163	100.27	4.9438	1.2987	20.57/79.43/0
LNCTO-1.25	2.8658	14.170	100.83	4.9443	1.2787	19.06/79.61/1.33
LNCTO-2.5	2.8665	14.177	100.81	4.9458	1.2582	17.74/79.65/2.61
LNCTO-5	2.8665	14.179	101.47	4.9463	1.2448	14.76/79.52/5.72

Using the obtained $LiNi_{0.8}Co_{0.2-x}Ti_xO_2$ samples as cathode materials, galvanostatic charging and discharging of 2032-type coin cells was carried out between 2.5 V and 4.3 V at different rates. The resultant charge–discharge curves, cycling performance, and rate capabilities are shown in Fig. 6. Moreover, the corresponding electrochemical results are presented in Table II. Similar curves were observed for all four samples (Fig. 6a–d), indicating the limited influence of Ti doping on the lithium insertion/extraction in such batteries.[20] The initial discharge capacities of the $LiNi_{0.8}Co_{0.2-x}Ti_xO_2$ samples decreased with increasing Ti doping amount (Table II), which may be because of the electrochemical inertness of the doped Ti^{4+}.[42,43] However, the discharge capacities of both LNCTO-1.25 (189 mAh g^{-1} and 182 mAh g^{-1}) and LNCTO-2.5 (177 mAh g^{-1} and 163 mAh g^{-1}) in the 50th and 100th cycles were larger than those of the LNCTO-0 sample (176 mAh g^{-1} and 154 mAh g^{-1}), respectively, indicating an improvement in the cycling stability upon doping appropriate amounts of Ti in the samples (Table II; Fig. 6e). Furthermore, the rate capability of both LNCTO-1.25 (162 mAh g^{-1}) and LNCTO-2.5 (160 mAh g^{-1}) was higher than that of LNCTO-0 (156 mAh g^{-1}) at 2C (Table II; Fig. 6f). This enhanced cycling stability and rate performance may be because of the improved lithium diffusion in the crystal structures after the cell volumes is slightly enlarged by doping Ti, as discussed regarding the XRD results.[31] As shown by the SEM results of the samples, the Ti-doped products displayed morphologies (microspheres) and secondary particle sizes (0.2 μm to 1.5 μm) similar to those of $LiNi_{0.8}Co_{0.2}O_2$ when the doping amount

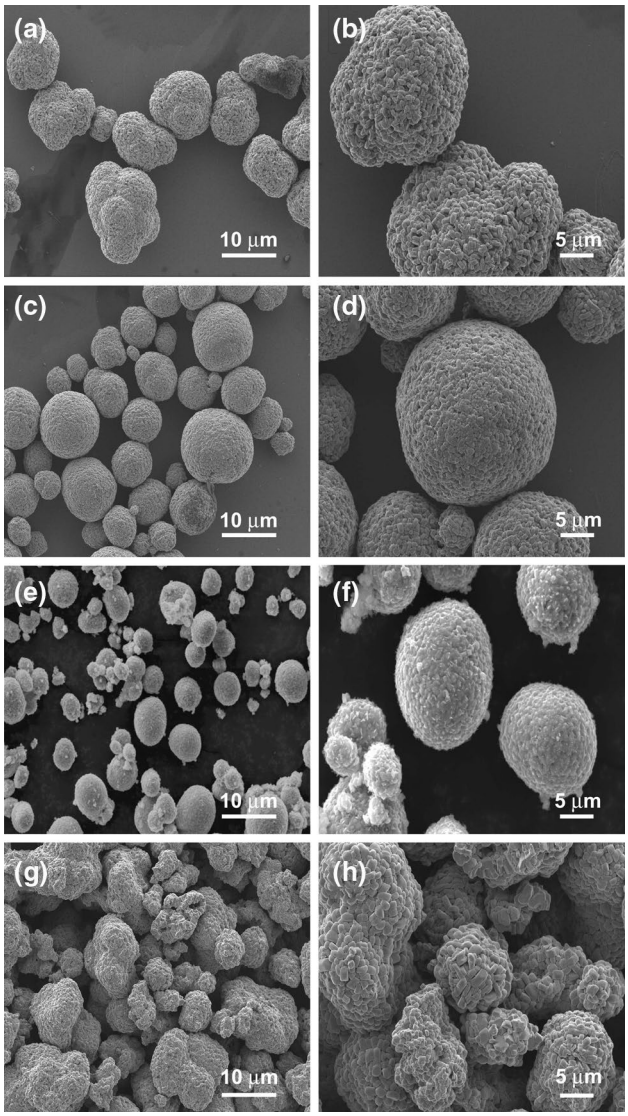

Fig. 3 SEM images of $LiNi_{0.8}Co_{0.2-x}Ti_xO_2$ cathode materials with (a, b) $x = 0$, (c, d) $x = 0.0125$, (e, f) $x = 0.025$, and (g, h) $x = 0.05$.

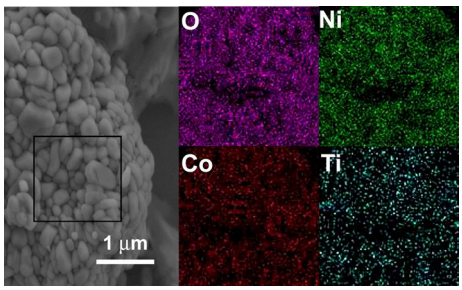

Fig. 4 EDX elemental mapping of O, Ni, Co, and Ti for LNCTO-1.25.

was low ($x \leq 0.025$), indicating the negligible effect of Ti doping on the product morphology. However, a significant difference in the electrochemical performance (including the cycling stability and rate performance) was found among the obtained $LiNi_{0.8}Co_{0.2-x}Ti_xO_2$ ($0 \leq x \leq 0.025$) samples, suggesting a weak correlation between sample morphology and electrochemical performance. In addition, when more Ti ($x = 0.05$) was doped into the sample (LNCTO-5), poor cycling stability (capacity retention of 76.5% upon 100 cycles) and low rate capability (141 mAh g^{-1} at 2C) were observed (Table II), which can be attributed to the severe Li^+/ Ni^{2+} cation mixing and enlarged secondary particles upon excess Ti entering the crystal lattice, as described regarding the XRD and SEM results.[40,41]

CV tests were carried out to investigate the effect of Ti doping on the electrochemical behavior of the $LiNi_{0.8}Co_{0.2-x}Ti_xO_2$ samples. Figure 7a–d depicts the first three CV cycles of four different $LiNi_{0.8}Co_{0.2-x}Ti_xO_2$ samples between 3.0 V and 4.6 V at 1 mV s^{-1}. As shown in Fig. 7a, compared with the second and third CV cycles of the $LiNi_{0.8}Co_{0.2}O_2$ sample, its first cycle showed an obviously different shape, which is because of the initial stabilization and solid-electrolyte interphase (SEI) formation in the first cycle.[49,50] Similar results were observed for the $LiNi_{0.8}Co_{0.2-x}Ti_xO_2$ samples with $x = 0.0125$ and 0.025. For all four $LiNi_{0.8}Co_{0.2-x}Ti_xO_2$ samples (x =0, 0.0125, 0.025, and 0.05), nearly overlapping curves are seen for the second and third cycles, indicating improved interfacial stability and electrochemical reversibility after the initial activation in the first cycle.[51] For LNCTO-0, LNCTO-1.25, and LNCTO-2.5, each of the CV curves exhibited three couples of oxidation and reduction peaks, including one sharp and two weak redox pairs (Fig. 7a-c), corresponding to the phase transitions of hexagonal phase (H1)/monoclinic phase (M), monoclinic phase (M)/hexagonal phase (H2), and hexagonal phase (H2)/hexagonal phase (H3) during lithium deintercalation and intercalation.[18,52] However, only one redox pair was observed when x was equal to 0.05 (Fig. 7d), indicating a reduction of the electrochemical activity with the introduction of excessive Ti due its electrochemical inertness in the crystal structure. The peak positions of the H1/M phase transitions (at 3.9 V to 4.1 V) and the corresponding potential differences (ΔV) are presented in Table III for LNCTO-0, LNCTO-1.25, and LNCTO-2.5. Compared with LNCTO-0, a decrease of ΔV for the LNCTO-1.25 and LNCTO-2.5 samples can be found. Therefore, doping with a proper amount of Ti was helpful to weaken the electrode polarization of $LiNi_{0.8}Co_{0.2}O_2$, which can improve the high-rate performance and cycle stability.[53,54]

To enable investigation of their resistance parameters and lithium-ion diffusion, Nyquist plots of the EIS results for the pristine and Ti-doped $LiNi_{0.8}Co_{0.2}O_2$ cathode materials are shown in Fig. 7e. The EIS curves of all four samples showed similar shapes, consisting of three semicircles from high- to intermediate-frequency regions and

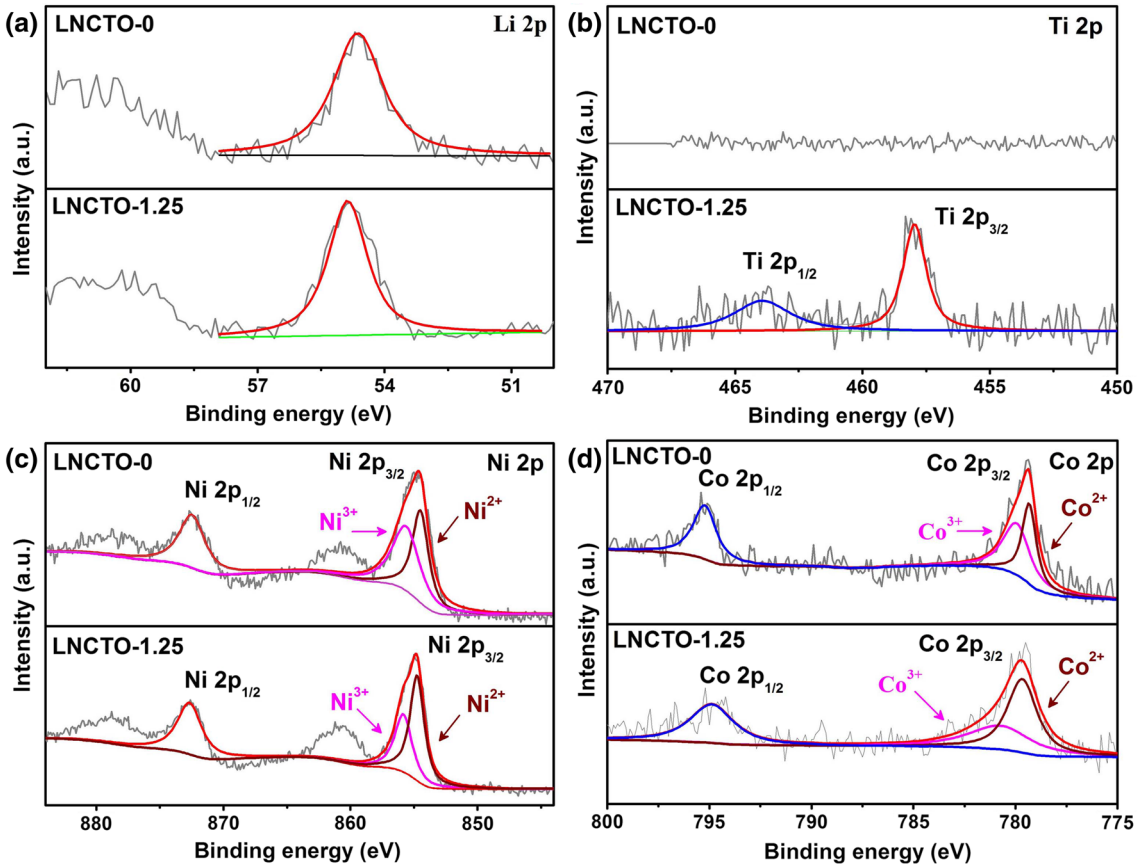

Fig. 5 XPS spectra of (a) Li 1*s*, (b) Ti 2*p*, (c) Ni 2*p*, and (d) Co 2*p*.

an inclined line in the low-frequency region. The three semicircles can be assigned to the surface-film resistance, electron transfer impedance, and charge-transfer impedance, respectively.[55,56] The inclined line can be associated with lithium-ion diffusion in the electrode, which is known as Warburg diffusion.[57] Compared with LNCTO-0, the decreased diameter of the semicircle for LNCTO-1.25, LNCTO-2.5, and LNCTO-5 indicates a reduction of the charge-transfer resistance and an improvement of the lithium-ion migration in the resultant electrode upon Ti doping.[58–60] As shown in the XRD results, Ti doping led to an increase of the *c*/*a* value for three $LiNi_{0.8}Co_{0.2-x}Ti_xO_2$ samples, implying an improvement of the layered crystal structure of the Ti-doped samples. Moreover, the cell volume was slightly enlarged upon Ti doping of $LiNi_{0.8}Co_{0.2}O_2$, leading to enlarged Li-ion transport channels and improved lithium diffusion in the Ti-doped crystal structures. Therefore, the EIS results indicate the decreased resistances of the Ti-doped samples compared with pristine $LiNi_{0.8}Co_{0.2}O_2$. However, the $I(003)/I(104)$ value increased with increasing Ti doping amount, indicating more serious cation mixing with more Ti doping. Cation mixing can block lithium diffusion and increase the resistance of cathode materials. As a result, the resistances of the Ti-doped samples were lowest for the LNCTO-1.25 sample.

Conclusions

Layered nickel-rich $LiNi_{0.8}Co_{0.2-x}Ti_xO_2$ (x=0, 0.0125, 0.025, and 0.05) materials with size of 5 μm to 10 μm were successfully synthesized by calcination of $Ni_{0.8}Co_{0.2-x}Ti_x(OH)_2$ precursors together with $LiOH{\cdot}H_2O$. The reversible capacity of $LiNi_{0.8}Co_{0.2-x}Ti_xO_2$ (x = 0.0125) was 182 mAh g^{-1} at 0.5C after 100 cycles, much higher than that of pristine $LiNi_{0.8}Co_{0.2}O_2$ (154 mAh g^{-1}). Moreover, the discharge capacity of $LiNi_{0.8}Co_{0.2-x}Ti_xO_2$ (x = 0.0125) was 200 mAh g^{-1}, 193 mAh g^{-1}, 182 mAh g^{-1}, and 162 mAh g^{-1} at 0.2C, 0.5C, 1C, and 2C, respectively, also being higher than those for pristine $LiNi_{0.8}Co_{0.2}O_2$ samples. To study the electrochemical behavior of $LiNi_{0.8}Co_{0.2-x}Ti_xO_2$, CV and EIS tests were carried out. The results indicated a reduced charge-transfer resistance, improved lithium-ion migration, and weakened electrode polarization of the layered structures upon Ti doping.

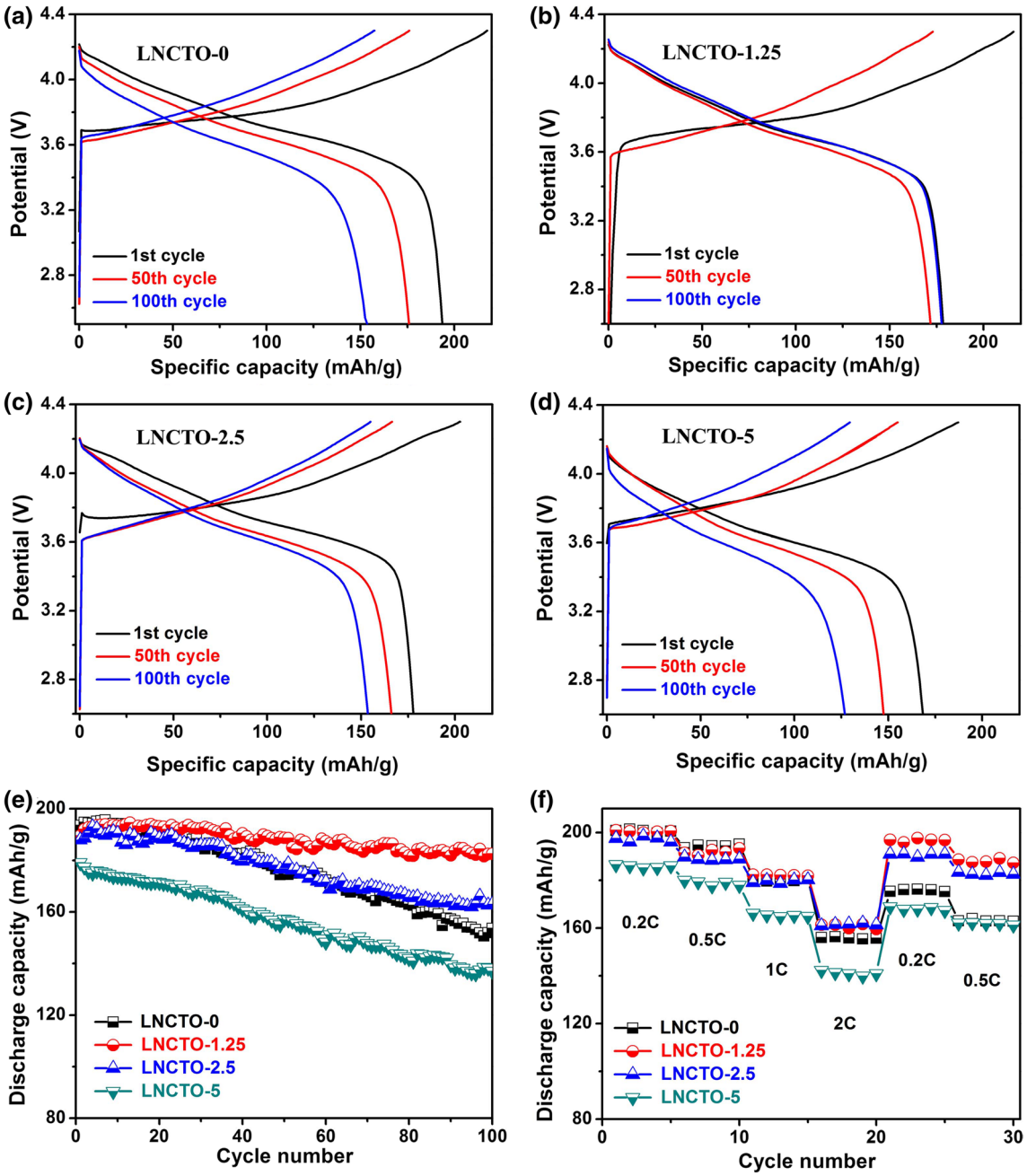

Fig. 6 Charge–discharge curves of 1st, 50th, and 100th cycles for $LiNi_{0.8}Co_{0.2-x}Ti_xO_2$ samples with (a) $x = 0$, (b) $x = 0.0125$, (c) $x = 0.025$, and (d) $x = 0.05$ at rate of 0.5 C. (e) Cycling performance at 0.5C and (f) rate capabilities obtained from 0.2C to 2C for the $LiNi_{0.8}Co_{0.2-x}Ti_xO_2$ samples.

Table II Electrochemical performance of $LiNi_{0.8}Co_{0.2-x}Ti_xO_2$ ($0 \le x \le 5\%$) samples

Sample	Cycling Performance (mAh g^{-1})			Capacity Retention (%)		Rate Capability (mAh g^{-1})			
	1st	50th	100th	50th	100th	0.2C	0.5C	1C	2C
LNCTO-0	194	176	154	90.7	79.4	201	194	179	156
LNCTO-1.25	190	189	182	99.5	95.8	200	193	182	162
LNCTO-2.5	188	177	163	94.1	86.7	198	188	179	160
LNCTO-5	179	157	137	87.7	76.5	185	178	165	141

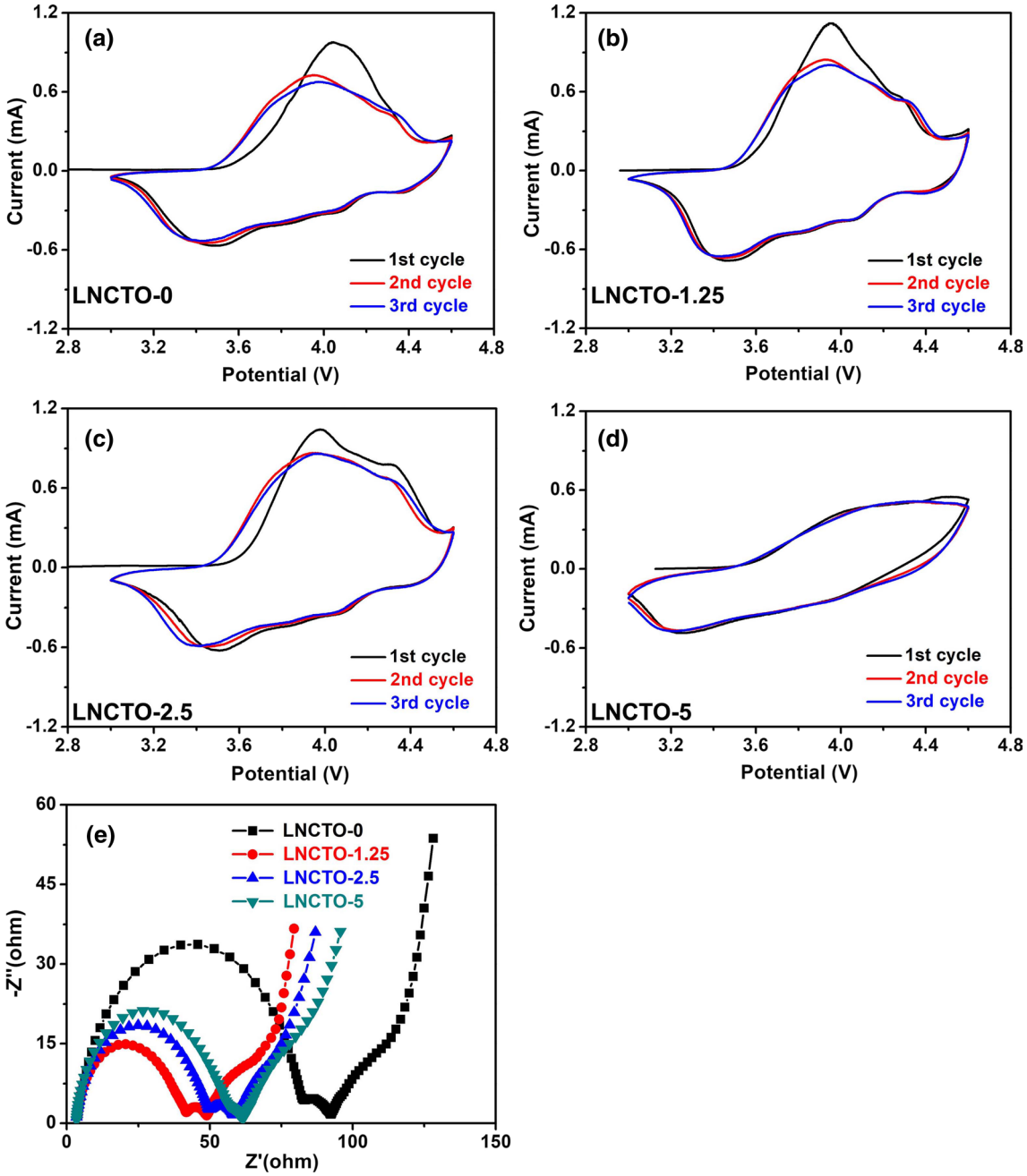

Fig. 7 CV curves of (a) LNCTO-0, (b) LNCTO-1.25, (c) LNCTO-2.5, and (d) LNCTO-5; (e) EIS results of four samples.

Table III Potential differences obtained from CV curves of LNCTO-0, LNCTO-1.25, and LNCTO-2.5

Sample	Cycle Number	Oxidation Peak (V)	Reduction Peak (V)	Potential Difference (V)
LNCTO-0	First	4.045	3.510	0.535
	Second	3.949	3.426	0.523
	Third	3.969	3.423	0.546
LNCTO-1.25	First	3.960	3.473	0.487
	Second	3.925	3.448	0.477
	Third	3.941	3.439	0.502
LNCTO-2.5	First	3.976	3.498	0.478
	Second	3.956	3.464	0.492
	Third	3.942	3.427	0.515

Funding This work is supported by Science and Technology Project of Guizhou Province (QKHCG[2021]YB104).

Conflict of interest The authors declare that they have no conflicts of interest.

References

1. J. Kim, H. Lee, H. Cha, M. Yoon, M. Park, and J. Cho, *Adv. Energy Mater.* 8, 1702028 (2018).
2. L. de Biasi, B. Schwarz, T. Brezesinski, P. Hartmann, J. Janek, and H. Ehrenberg, *Adv. Mater.* 31, 1900985 (2019).
3. M. Li, J. Liu, T. Liu, M. Zhang, and F. Pan, *Chem. Commun.* 54, 1331 (2018).
4. J.M. Tarascon, and M. Armand, *Nature* 414, 359 (2001).
5. M. Winter, J.O. Besenhard, M.E. Spahr, and P. Novak, *Adv. Mater.* 10, 725 (1998).
6. J. Cho, *Chem. Mater.* 12, 3089 (2000).
7. S. Venkatraman, Y. Shin, and A. Manthiram, *Electrochem. Solid State Lett.* 6, A9 (2003).
8. J.R. Ying, C.R. Wan, C.Y. Jiang, and Y.X. Li, *J. Power Sources* 99, 78 (2001).
9. G.T.K. Fey, V. Subramanian, and C.Z. Lu, *Solid State Ionics* 152, 83 (2002).
10. T.H. Cho, and H.T. Chung, *J. Appl. Electrochem.* 35, 1033 (2005).
11. Z. Yang, B. Wang, W. Yang, and X. Wei, *Electrochim. Acta* 52, 8069 (2007).
12. J. Xie, X. Huang, Z. Zhu, and J. Dai, *Ceram. Int.* 37, 665 (2011).
13. Y.H. Jouybari, and S. Asgari, *J. Power Sources* 196, 337 (2011).
14. H. Jia, W. Zhu, Z. Xu, X. Nie, T. Liu, L. Gao, and J. Zhao, *Electrochim. Acta* 266, 7 (2018).
15. K. Nishio, K. Horiba, N. Nakamura, M. Kitamura, H. Kumigashira, R. Shimizu, and T. Hitosugi, *J. Power Sources* 416, 56 (2019).
16. D.P. Abraham, R.D. Twesten, M. Balasubramanian, I. Petrov, J. McBreen, and K. Amine, *Electrochem. Commun.* 4, 620 (2002).
17. K. Nikolowski, N.N. Bramnik, C. Baehtz, H. Ehrenberg, and H. Fuess, *J. Power Sources* 174, 818 (2007).
18. J. Zhao, W. Zhang, A. Huq, S.T. Misture, B. Zhang, S. Guo, L. Wu, Y. Zhu, Z. Chen, K. Amine, F. Pan, J. Bai, and F. Wang, *Adv. Energy Mater.* 7, 1601266 (2017).
19. W.-S. Yoon, K.-W. Nam, D. Jang, K.Y. Chung, J. Hanson, J.-M. Chen, and X.-Q. Yang, *J. Power Sources* 217, 128 (2012).
20. X. Yang, Y. Tang, Y. Qu, G. Shang, J. Wu, J. Zheng, Y. Lai, J. Li, and Z. Zhang, *J. Power Sources* 438, 226978 (2019).
21. W. Kang, G. Jia, X. Shangguan, G. Yang, Z. Zhu, Z. Peng, Z. Qin, F. Li, and X. Cui, *J. Alloys Compd.* 765, 700 (2018).
22. G.T.K. Fey, J.G. Chen, V. Subramanian, and T. Osaka, *J. Power Sources* 112, 384 (2002).
23. M. Choi, K. Kang, H.-S. Kim, Y.M. Lee, and B.-S. Jin, *RSC Adv.* 5, 4872 (2015).
24. H. Qiu, H. Yue, X. Wang, T. Zhang, M. Zhang, Z. Fang, X. Zhao, G. Chen, Y. Wei, C. Wang, and D. Zhang, *J. Alloys Compd.* 725, 860 (2017).
25. Z. Hua, X. Zhang, X. Feng, X. Wang, J. He, X. Wang, and H. Peng, *Chin. Chem. Lett.* 30, 792 (2019).
26. X. Sun, Y. Xu, G. Chen, P. Ding, and X. Zheng, *Solid State Ionics* 268, 236 (2014).
27. J.-H. Song, J. Bae, K.-W. Lee, I. Lee, K. Hwang, W. Cho, S.J. Hahn, and S. Yoon, *J. Ind. Eng. Chem.* 68, 124 (2018).
28. J. Li, M. Liu, J. An, P. Tian, C. Tang, T. Jia, F.K. Butt, D. Yu, W. Bai, C. Cao, and X. Feng, *J. Alloys Compd.* 829, 1545 (2020).
29. A. Nurpeissova, M.H. Choi, J.-S. Kim, S.-T. Myung, S.-S. Kim, and Y.-K. Sun, *J. Power Sources* 299, 425 (2015).
30. H. Yang, H.-H. Wu, M. Ge, L. Li, Y. Yuan, Q. Yao, J. Chen, L. Xia, J. Zheng, Z. Chen, J. Duan, K. Kisslinger, X.C. Zeng, W.-K. Lee, Q. Zhang, and J. Lu, *Adv. Funct. Mater.* 29, 1808825 (2019).
31. H. Sun, Z. Cao, T. Wang, R. Lin, Y. Li, X. Liu, L. Zhang, F. Lin, Y. Huang, and W. Luo, *Mater. Today Energy* 13, 145 (2019).
32. M. Xiang, W. Tao, J. Wu, Y. Wang, and H. Liu, *Ionics* 22, 1003 (2016).
33. D. Kong, J. Hu, Z. Chen, K. Song, C. Li, M. Weng, M. Li, R. Wang, T. Liu, J. Liu, M. Zhang, Y. Xiao, and F. Pan, *Adv. Energy Mater.* 9, 1901756 (2019).
34. J.P. Cho, and B. Park, *J. Power Sources* 92, 35 (2001).
35. H.S. Liu, J. Li, Z.R. Zhang, Z.L. Gong, and Y. Yang, *Electrochim. Acta* 49, 1151 (2004).
36. Y. Idemoto, A. Horie, N. Ishida, and N. Kitamura, *Electrochemistry* 84, 802 (2016).
37. X. Cao, L. Xie, and R. Wang, *J. Solid State Electrochem.* 15, 473 (2011).
38. P. Liu, L. Xiao, Y. Chen, and H. Chen, *Ceram. Int.* 45, 18398 (2019).
39. Y.-D. Xu, W. Xiang, Z.-G. Wu, C.-L. Xu, Y.-C. Li, X.-D. Guo, G.-P. Lv, X. Peng, and B.-H. Zhong, *Electrochim. Acta* 268, 358 (2018).
40. Y. Wang, J. Roller, and R. Maric, *Electrochim. Acta* 241, 510 (2017).
41. S. Zhong, M. Lai, W. Yao, and Z. Li, *Electrochim. Acta* 212, 343 (2016).
42. J. Kim, and K. Amine, *J. Power Sources* 104, 33 (2002).
43. Y. Cho, S. Lee, Y. Lee, T. Hong, and J. Cho, *Adv. Energy Mater.* 1, 821 (2011).
44. X. Yang, R. Yu, L. Ge, D. Wang, Q. Zhao, X. Wang, Y. Bai, H. Yuan, and H. Shu, *J. Mater. Chem. A* 2, 8362 (2014).
45. M. Rastgoo-Deylami, M. Javanbakht, and H. Omidvar, *Solid State Ionics* 331, 74 (2019).
46. F. Wu, J. Tian, Y. Su, J. Wang, C. Zhang, L. Bao, T. He, J. Li, and S. Chen, *ACS Appl. Mater. Interfaces* 7, 7702 (2015).
47. L. Zhu, G. Yang, J. Liu, C. Bao, L. Xie, and X. Cao, *ChemistrySelect* 4, 11475 (2019).
48. D.A. Anang, J.-H. Park, D.S. Bhange, M.K. Cho, W.Y. Yoon, K.Y. Chung, and K.-W. Nam, *Ceram. Int.* 45, 23164 (2019).
49. H. Yin, X.-X. Yu, H. Zhao, C. Li, and M.-Q. Zhu, *J. Solid State Electrochem.* 22, 2395 (2018).
50. R. Robert, C. Buenzli, E.J. Berg, and P. Novak, *Chem. Mater.* 27, 526 (2015).

51. Z.X. Wang, Y.C. Sun, L.Q. Chen, and X.J. Huang, *J. Electrochem. Soc.* 151, A914 (2004).
52. E. Han, X. Du, P. Yang, and Y. Han, *Ionics* 24, 393 (2018).
53. Y. Huang, X. Yao, X. Hu, Q. Han, S. Wang, L.-X. Ding, and H. Wang, *Appl. Surf. Sci.* 489, 913 (2019).
54. Y.-J. Huang, D.-S. Gao, G.-T. Lei, Z.-H. Li, and G.-Y. Su, *Mater. Chem. Phys.* 106, 354 (2007).
55. Y. Zhou, X. Hou, K. Shen, S. Wang, F. Chen, Y. Li, H. Chen, and B. Wang, *Ionics* 25, 51 (2019).
56. P.-C. Tsai, B. Wen, M. Wolfman, M.-J. Choe, M.S. Pan, L. Su, K. Thornton, J. Cabana, and Y.-M. Chiang, *Energy Environ. Sci.* 11, 860 (2018).
57. J. Liu, B. Reeja-Jayan, and A. Manthiram, *J. Phys. Chem. C* 114, 9528 (2010).
58. L.P. He, K. Li, Y. Zhang, and J. Liu, *ACS Appl. Mater. Interfaces* 12, 28253 (2020).
59. F.K. Li, Z.B. Liu, J.D. Shen, X.J. Xu, L.Y. Zeng, Y. Li, D.C. Zhang, S.Y. Zuo, and J. Liu, *Nanomaterials* 10, 2495 (2020).
60. F.K. Li, Z.B. Liu, J.D. Shen, X.J. Xu, L.Y. Zeng, B.H. Zhang, H. Zhu, Q. Liu, J. Liu, and M. Zhu, *J. Mater. Chem. A* 9, 2830 (2021).